Supplementary Information for *Abrupt loss and uncertain recovery from fires of Amazon forests under low climate mitigation scenarios*

Isabel Martínez Cano[1*], Elena Shevliakova[2], Sergey Malyshev[2], Jasmin John[2,3], Yan Yu[4], Benjamin Smith[5,6] and Stephen W. Pacala[1]

[1]Department of Ecology and Evolutionary Biology, Princeton University, Princeton, NJ 08544, USA

[2]NOAA/OAR/Geophysical Fluid Dynamics Laboratory, 201 Forrestal Road, Princeton, NJ 08540, USA

[3]NOAA/OAR/Atlantic Oceanographic and Meteorological Laboratory, Miami, FL, 33149 USA

[4]Department of Atmospheric and Oceanic Sciences, School of Physics, Peking University, China

[5]Department of Physical Geography and Ecosystem Science, Lund University, Lund, Sweden

[6]Hawkesbury Institute for the Environment, Western Sydney University, Penrith, NSW, Australia

**Corresponding author*: Isabel Martínez Cano (isamcano@gmail.com)

The SI contains 2 Supplementary Tables, 25 Supplementary Figures, 2 Supplementary Text and Supplementary References.

Table S1. List of CMIP6 ESMs included in the analyses of projected fires and biomass changes for the Amazon. The table provides references to locate the specific data and details the resolution of the land model component and the characteristics of the fire and dynamic global vegetation (DGV) models.

Source ID	Institution ID	Nominal Resolution (km)	Variant Label	Fire Model	DGVM	Land Model
CESM2[1]	NCAR	100	r1i1p1f1 r2i1p1f1 r4i1p1f1	• Interactive natural fires based on refs. [2,3] • Daily fires burn biomass and kill vegetation, altering the canopy thickness and height[2]	• Vegetation distribution prescribed (prognostic vegetation state) • Fixed carbon allocation scheme	CLM5[4]
NorESM2-LM[5]	NCC	250	r1i1p1f1 r2i1p1f1 r3i1p1f1	• Same as CESM2	• Same as CESM2	CLM[4]
CNRM-ESM2-1[6]	CNRM-CERFACS	250	r1i1p1f2 r2i1p1f2 r3i1p1f2	• Interactive natural fires[7] based on ref.[8] • Daily fires decrease plant biomass	• No • Canopy represented by a single vegetation layer	SURFEXv8.0 (ISBA)[9]
EC-Earth3-Veg[10]	EC-Earth-Consortium	100	r1i1p1f1 r2i1p1f1 r3i1p1f1	• Interactive natural fires based on ref.[8] • Annual fires result in partial destruction of the biomass of an affected patch	• Yes • Cohort based vegetation dynamics (multi-layer canopy)	LPJ-GUESS v4[11,12]
GFDL-ESM4[13,14]	NOAA-GFDL	100	r1i1p1f1 r2i1p1f1 r3i1p1f1	• FINAL v2[(15,16)] • Daily fires affect the biomass and abundance of plant cohorts • New disturbed tiles formed following fires	• Yes • Cohort based vegetation dynamics (multi-layer energy balance)	LM4.1[17,18]
MRI-ESM2-0[19]	MRI	100	r1i1p1f1 r1i2p1f1 r1i3p1f1	—	• No	HAL 1.0[20]

Table S2. CMIP6 ESMs included in the analysis of trends in precipitation under scenario SSP5-8.5 for the Amazon.

Source ID	Institution ID	Nominal Resolution (km)	Variant Label
ACCESS-CM2	CSIRO-ARCCSS	250	r1i1p1f1
ACCESS-ESM1-5	CSIRO	250	r1i1p1f1
BCC-CSM2-MR	BCC	100	r1i1p1f1
CanESM5	CCCma	500	r1i1p1f1
CESM2	NCAR	100	r1i1p1f1
CESM2-WACCM	NCAR	100	r1i1p1f1
CNRM-CM6-1	CNRM-CERFACS	250	r1i1p1f2
CNRM-ESM2-1	CNRM-CERFACS	250	r1i1p1f2
EC-Earth3	EC-Earth-Consortium	100	r1i1p1f1
EC-Earth3-Veg	EC-Earth-Consortium	100	r1i1p1f1
FGOALS-f3-L	CAS	100	r1i1p1f1
FGOALS-g3	CAS	250	r1i1p1f1
GFDL-ESM4	NOAA-GFDL	100	r1i1p1f1
IPSL-CM6A-LR	IPSL	250	r1i1p1f1
KACE-1-0-G	NIMS-KMA	250	r1i1p1f1
MIROC6	MIROC	250	r1i1p1f1
MPI-ESM1-2-HR	DKRZ	100	r1i1p1f1
MPI-ESM1-2-LR	MPI-M	250	r1i1p1f1
MRI-ESM2-0	MRI	100	r1i1p1f1
NorESM2-LM	NCC	250	r1i1p1f1
NorESM2-MM	NCC	100	r1i1p1f1

Fig. S1. (a) Time series of tropical carbon gains (Mg C ha^{-1} y^{-1}). The green line shows reconstructed carbon gains (mean ± 95% CI) based on intact forest plot census data for the Amazon basin[21]. GFDL-ESM4.1 predictions (grey dots and dashed line) are based on annual averages of vegetation biomass in natural tropical forests during historical simulation experiments. (b) Observed vs. simulated patterns of AGB (Mg C ha^{-1}) across tropical forest sites. Observed stand level AGB estimates were retrieved from the database in ref. (22) for the tropics (see *Methods*). Aligned GFDL-ESM4.1 predictions correspond to averages over 2010-2014 for the corresponding grid cell locations. (c) Tree size distribution in the 50-ha census plot at Barro Colorado Island (BCI). The graph shows normalized tree abundance in a double logarithmic scale. The size distribution based on field data corresponds to the 2010 BCI census (green dots). GFDL-ESM4.1 predictions are based on averages over 2010-2014 (grey dots and line).

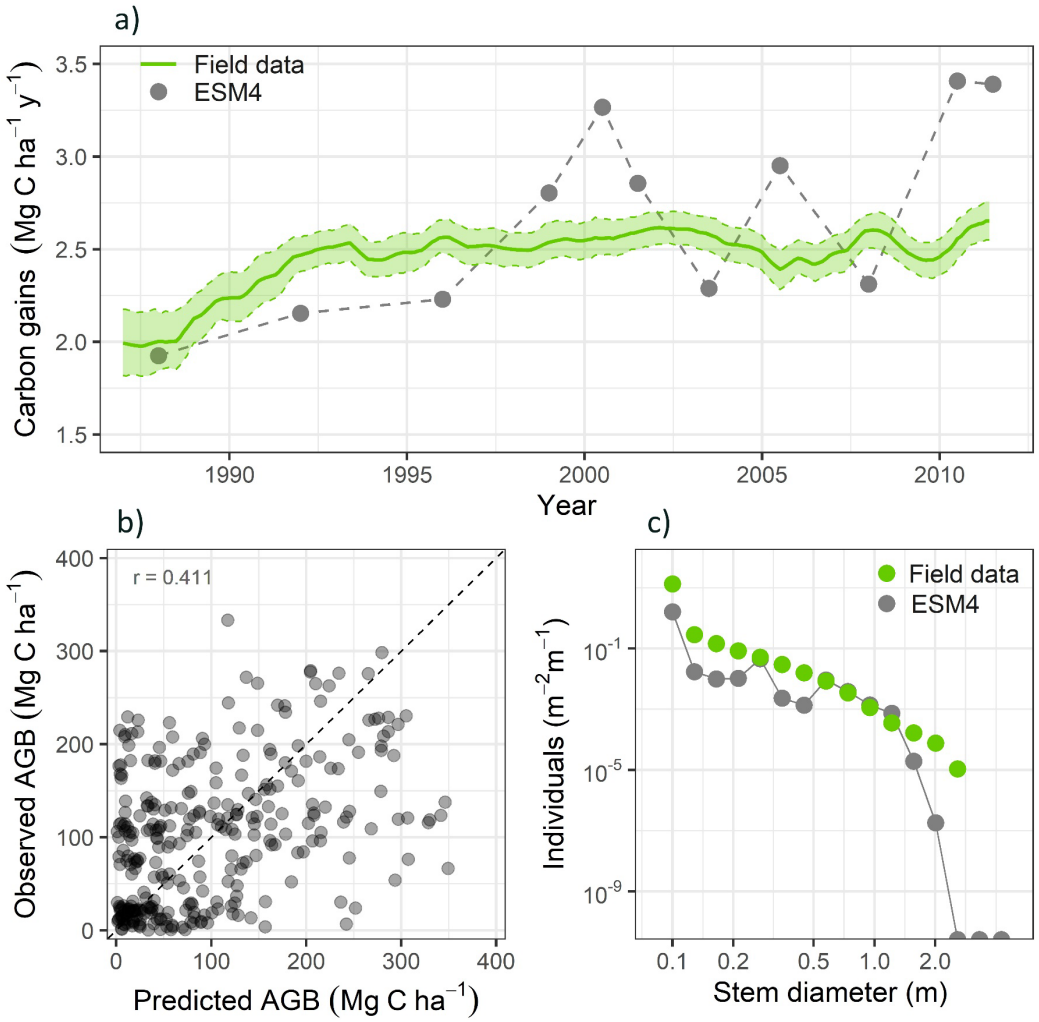

Fig. S2. Projected trends in normalized biomass based on GFDL-ESM4.1 global simulations under emission scenarios SSP1-2.6, SSP2-4.5, SSP3-7.0 and SSP5-8.5 for the Neotropics (tropical Americas) and Paleotropics (tropical areas of Africa and Asia). Annual biomass time series were normalized by dividing each value by the initial biomass for each realm to ease the comparison of predictions across experiments.

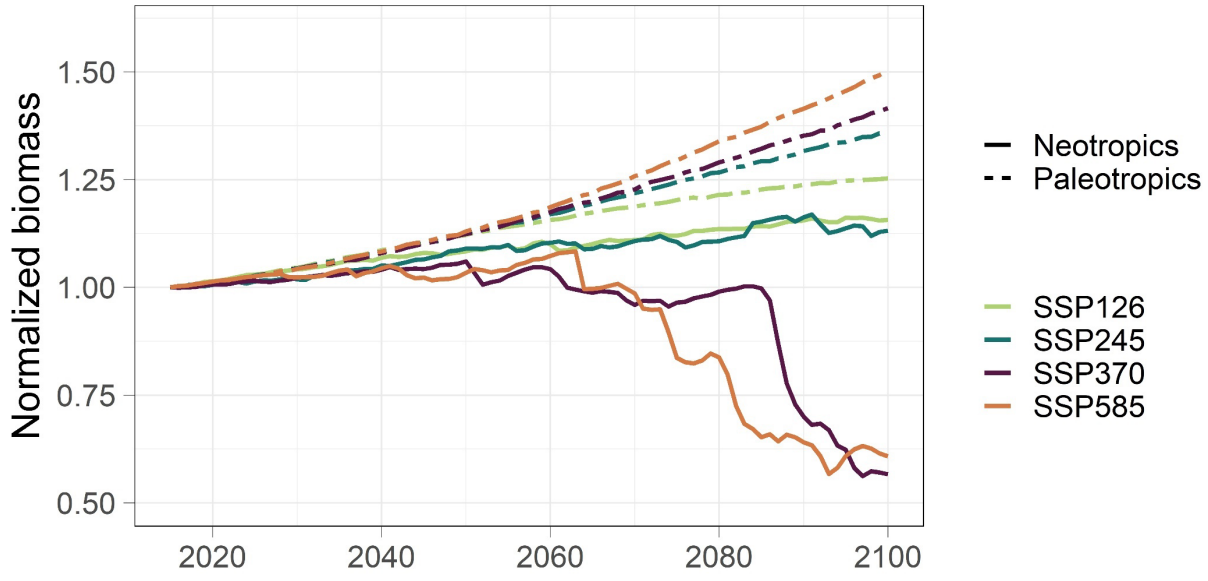

Fig. S3. Projected time series of mean annual total tree biomass (Kg C m^{-2}) in the Neotropics based on GFDL-ESM4.1 global simulations under CMIP6 historical (1850-2014) and future emission scenarios SSP1-2.6 and SSP5-8.5 (2015-2100). Each line corresponds to the dynamics of natural tropical forests in individual grid cell locations showing a decrease in forest biomass under scenario SSP5-8.5.

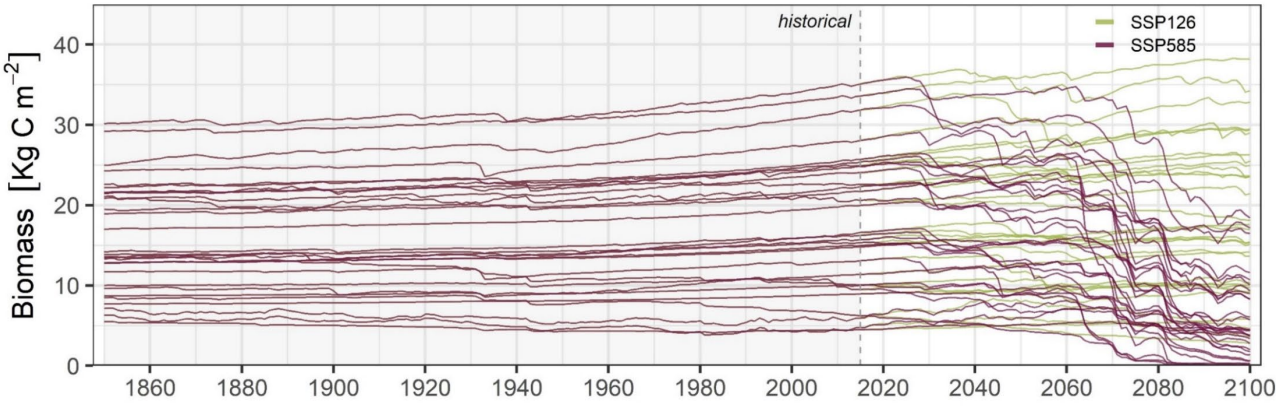

Fig. S4. Alternative version of Figure 2B in the main text, projected time series of mean annual total tree biomass (Kg C m^{-2}) in the Neotropics based on GFDL-ESM4.1 global simulations under future emission scenarios SSP1-2.6 and SSP5-8.5 (2015-2100). Each line corresponds to the dynamics of natural tropical forests in individual grid cell locations. Here, the color of each line maps to the simulated Mean Annual Precipitation (MAP) experienced on each location. Orange lines (rug) along the abscissa indicate years with high carbon emissions due to fires.

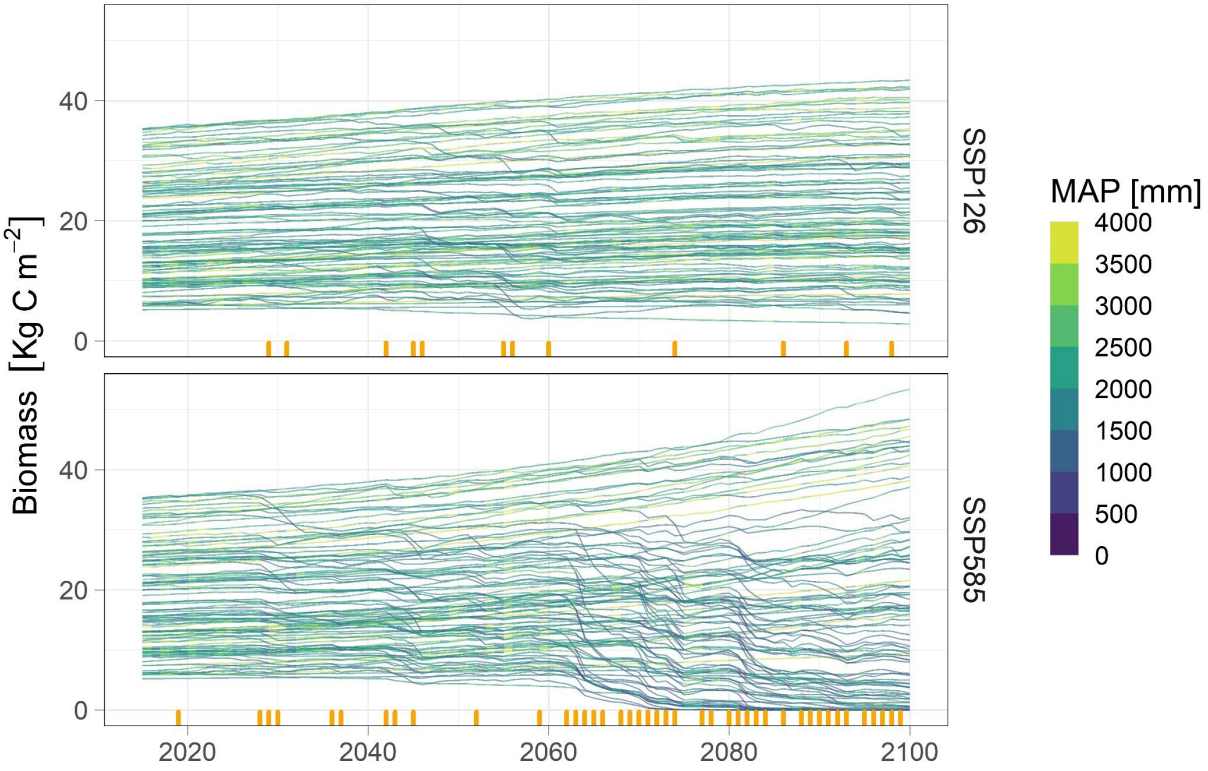

Fig. S5. Alternative version of Figure 2C in the main text, showing the simulated trajectories of each grid cell on tree biomass-MAP coordinates between 2015 and 2100 under scenario SSP5-8.5. Otherwise, same conventions as in Fig. 2C in the main text; green and purple dots corresponds to grid cells increasing or decreasing in tree biomass during the simulation. The reference lines represent the probability of different vegetation types (treeless, savanna, forest) estimated by ref. (10) based on remote sensing observations of vegetation cover and precipitation over South America. The background grey area delimits a bistability zone where the probability that forest is the dominant vegetation type is between 0.1 and 0.9.

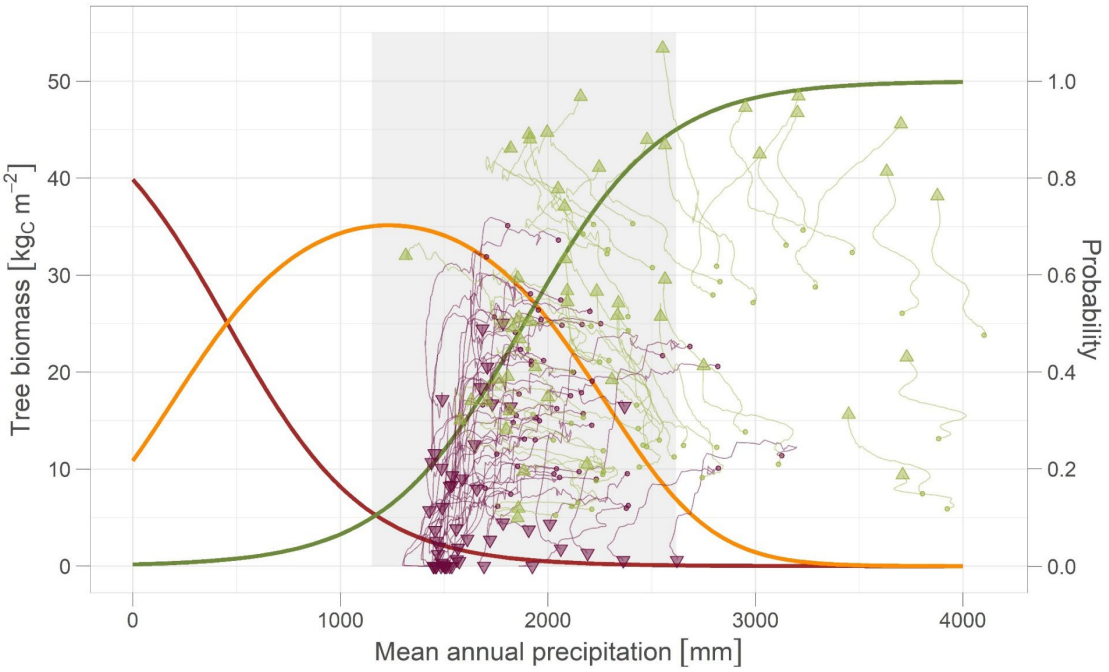

Fig. S6. Time series of fire suppression factors projected by GFDL-ESM4.1under SSP5-8.5 for Amazon cell locations. Each line corresponds to an individual grid cell covered by natural tropical forests. The last panel represents the probability of an ignition becomes a fire, p_{fire} (i.e., the product of all fire factors).

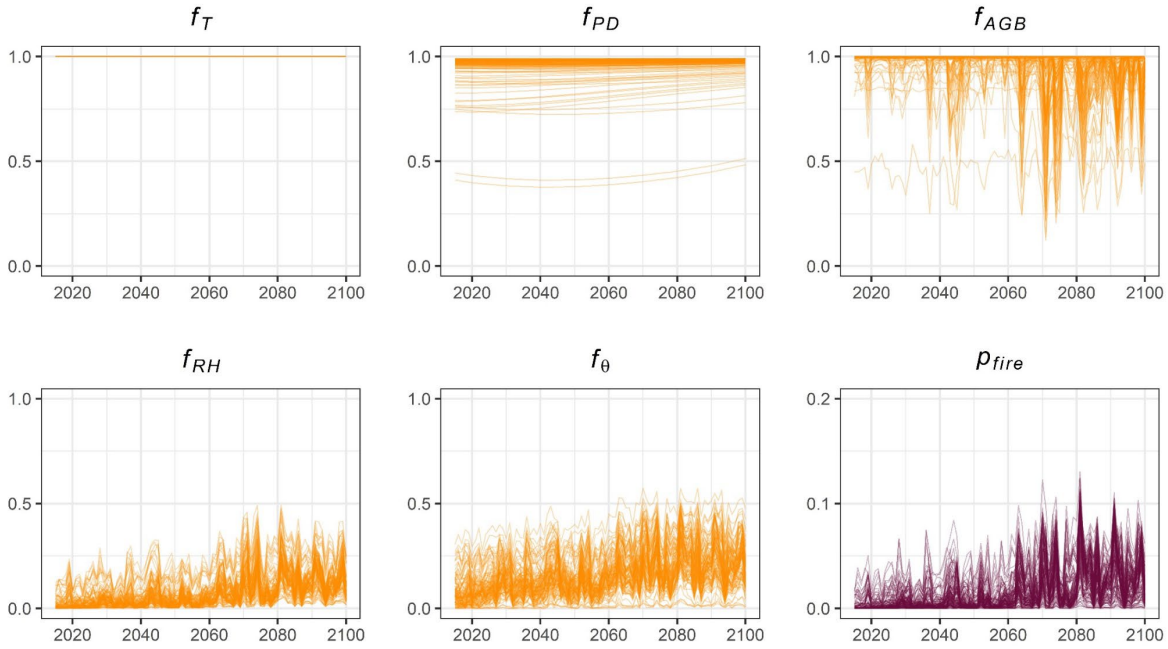

Fig. S7. Trends in precipitation (Oct–Mar average) in CMIP6 ESMs projections under SSP5-8.5 (2015-2100).

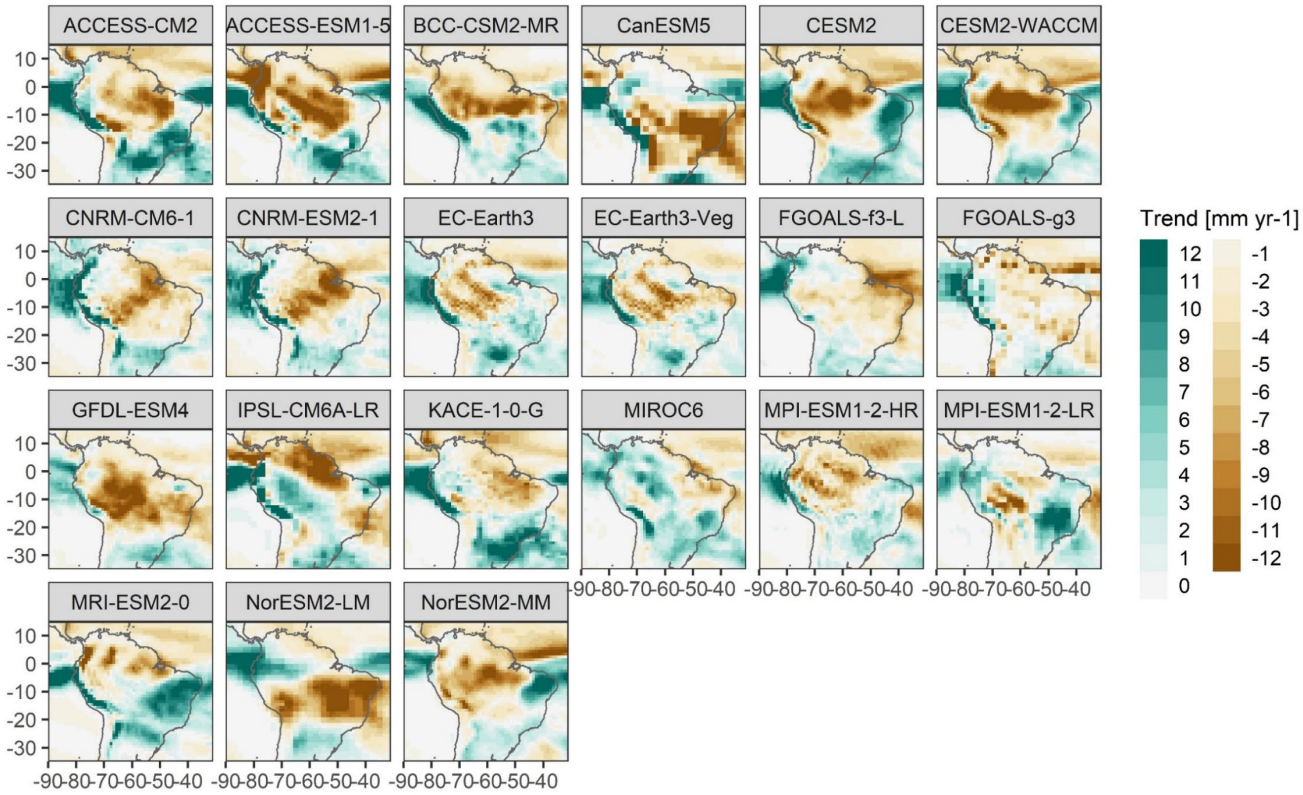

Fig. S8. Projected precipitation (Oct–Mar average) by CMIP6 ESMs at the start of the SSP5-8.5 experiment (2015).

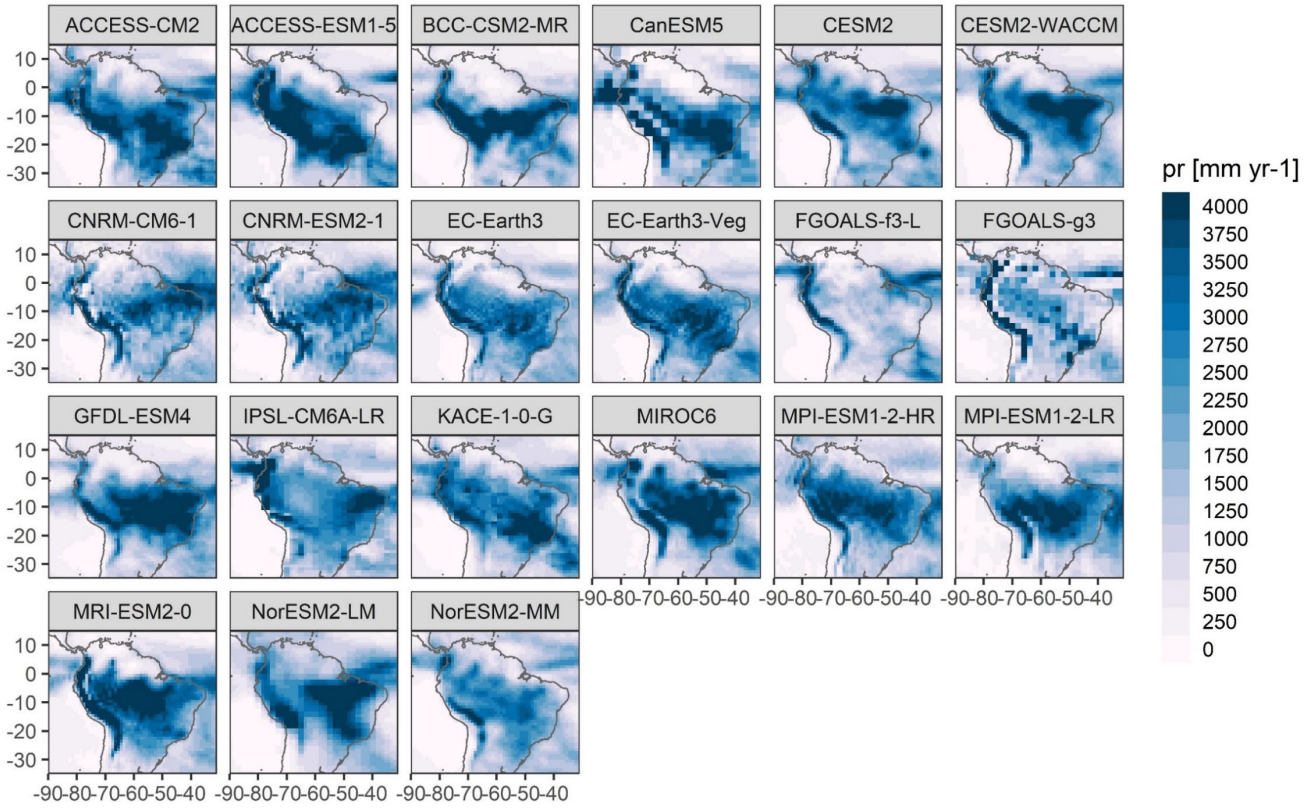

Fig. S9. Trends in precipitation over the Amazon (76ºW12ºN, 55ºW3ºS), smoothed with a 10 year window. The dashed grey line corresponds to the ensemble average across models. Mean precipitation at the start of the simulation (2015), and the linear trend (2015 to 2100) are detailed for each model in the upper right corner.

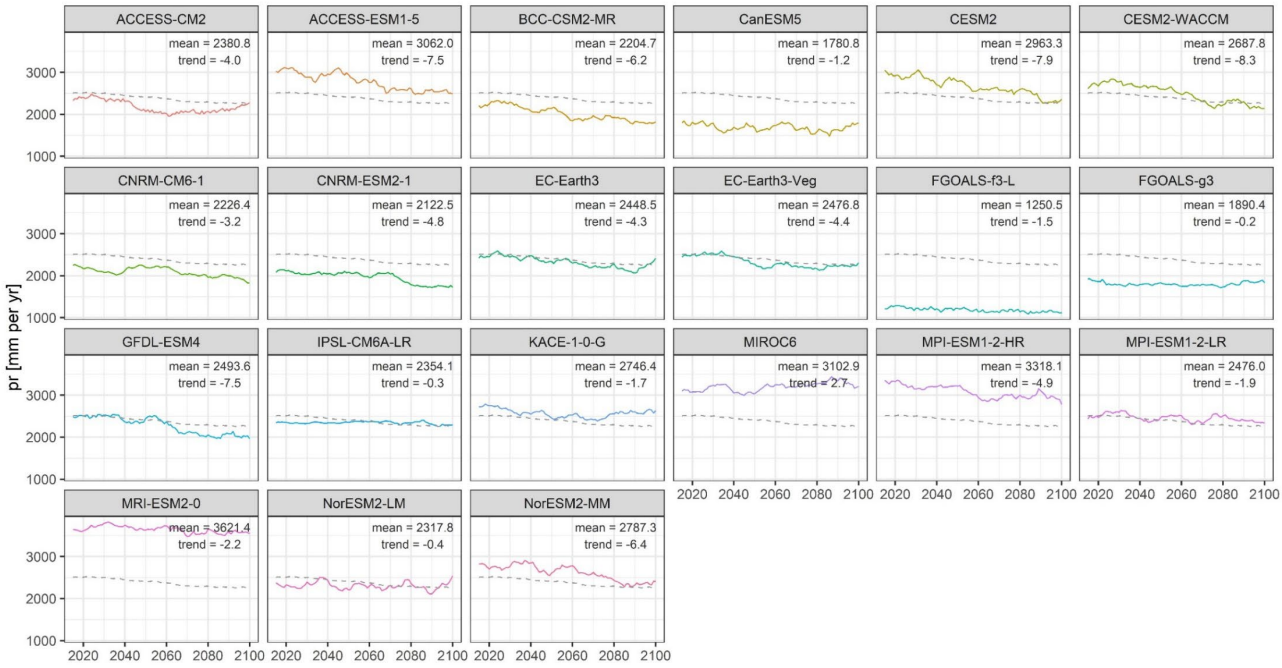

Fig. S10. Distribution of the rate of release of carbon lost through fires to the atmosphere (fire carbon emission, kg C m^{-2} yr^{-1}) in a climate space defined by annual mean temperature and precipitation. Different panels correspond to (a) estimates of fire emissions derived from remote sensing data (GFED4s, 1997-2014) and temperature and precipitation reanalysis data (Berkley Earth and NOAA GPCC, see *Methods*), and to GFDL-ESM4.1 simulations for (b) the historical period (1997-2014) and (c and d) future climate change scenarios SSP1-2.6 and SSP5-8.5 (2031-2050). Each dot corresponds to a tropical grid cell and year. The green dots in the background correspond to low smoke rates (smoke rate < 0.1).

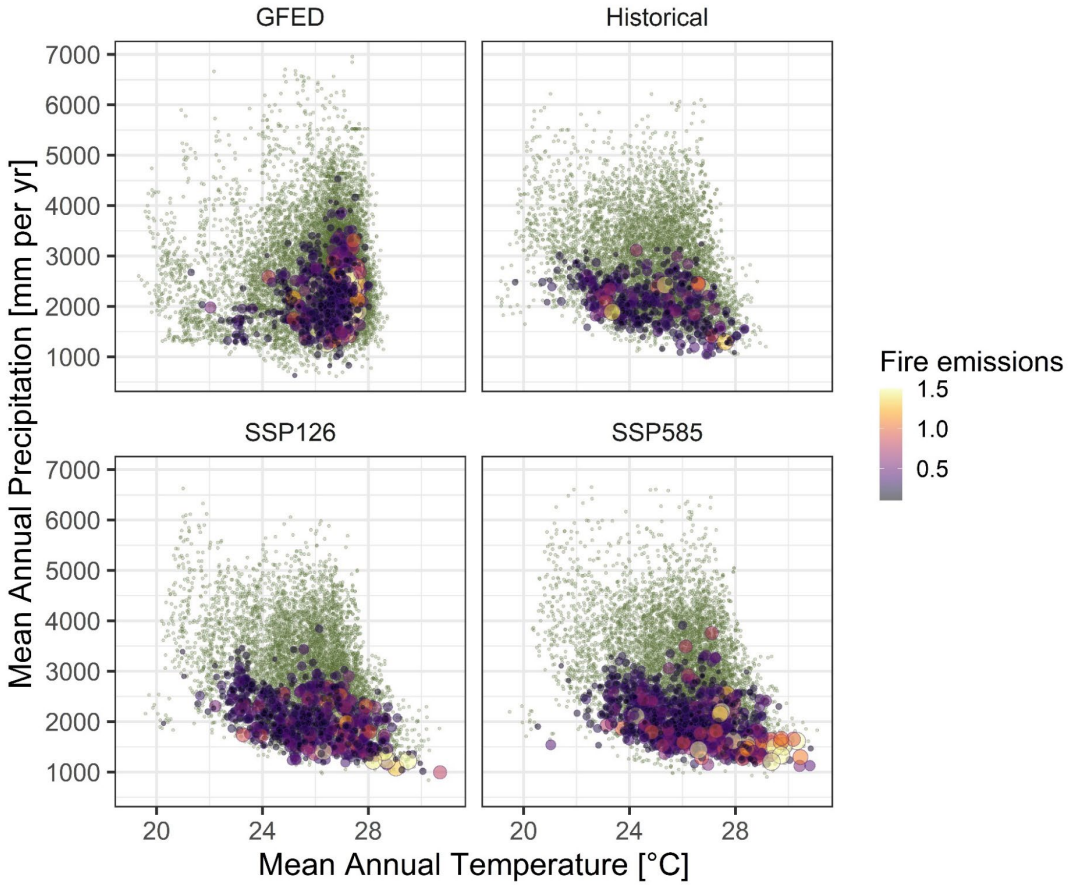

Fig. S11. Comparison of the rate of release of carbon lost through fire to the atmosphere (fire carbon emissions, kg C m^{-2} yr^{-1}) in (a) GFED4s estimates based on remote sensing and (b) GFDL-ESM4.1 simulations averaged during the period (1997-2014), and c) the absolute difference between both fields (RMSE = 0.0897). Means (standard deviations) are detailed in the upper right corner.

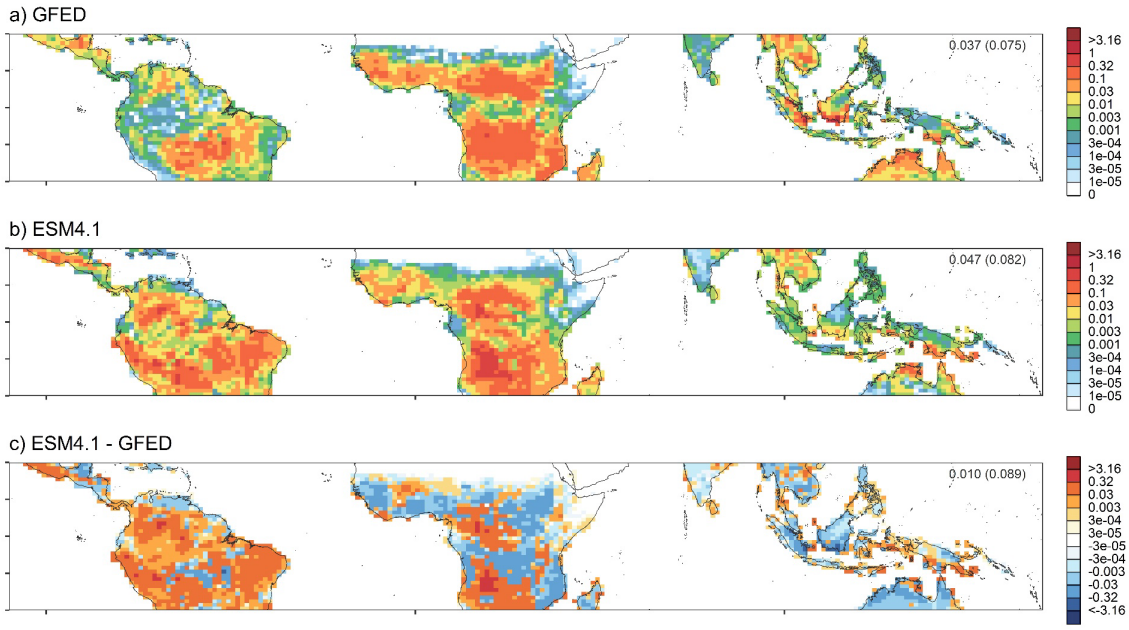

Fig. S12. Comparison of burned area fraction in (a) GFED4s estimates based on remote sensing and (b) GFDL-ESM4.1 simulations averaged during the period (1997-2014), and c) the absolute difference between both fields (RMSE = 0.0130). Means (standard deviations) are detailed in the upper right corner.

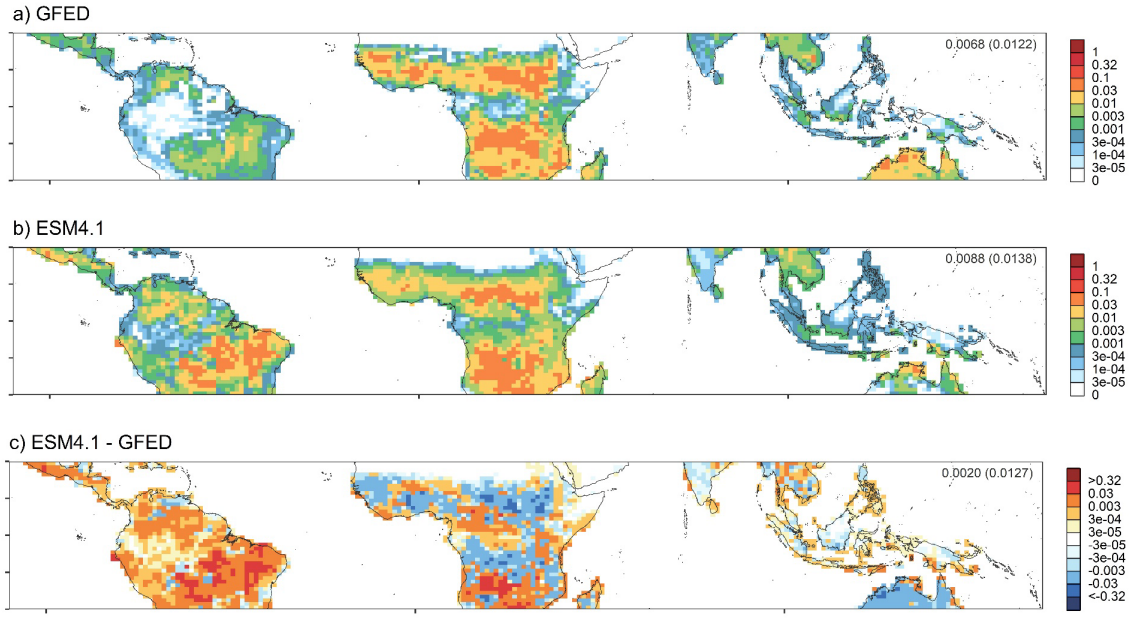

Fig. S13. Same as Figure S11C but showing the differences in carbon emissions due to fires between CMIP6 ESMs and GFED estimates.

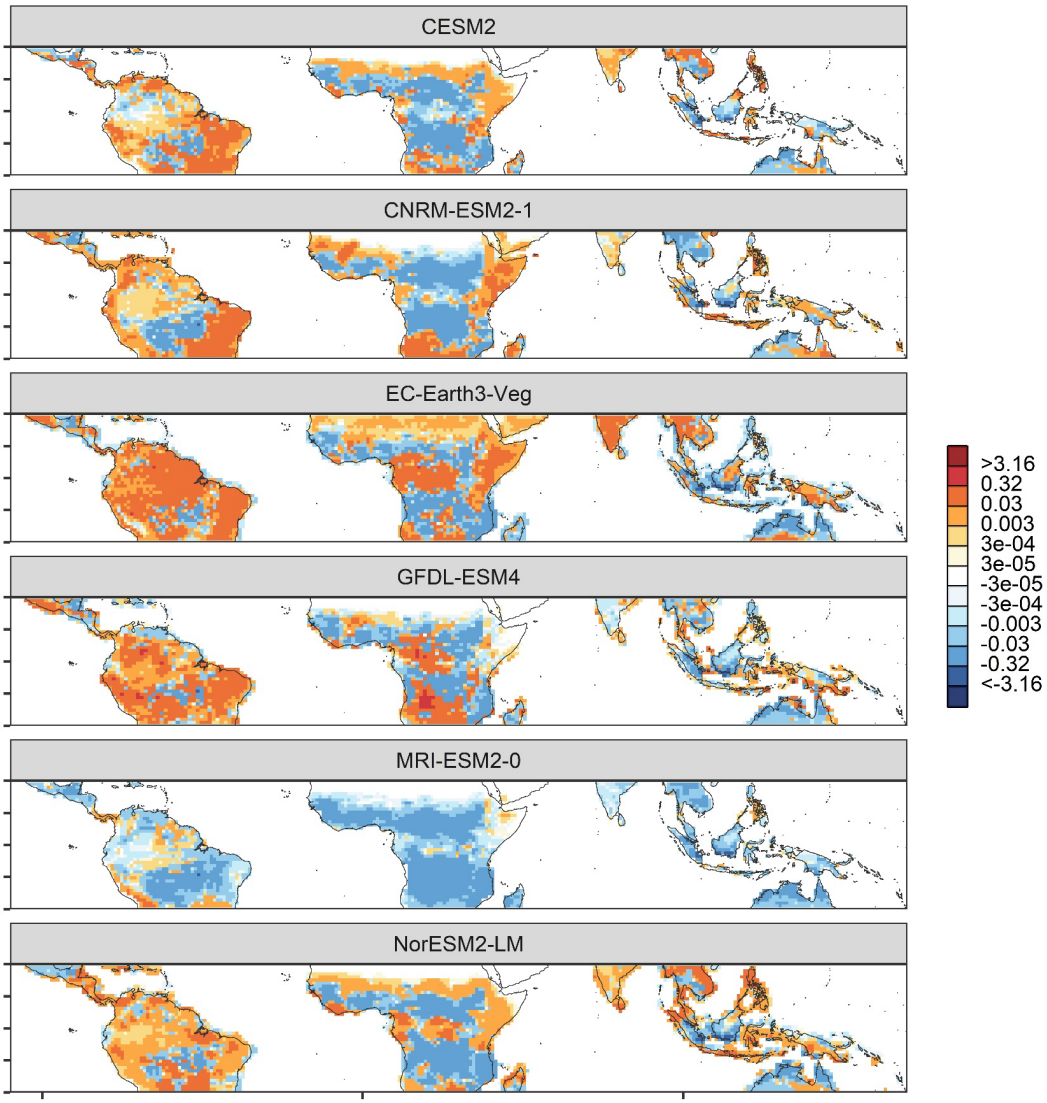

Fig. S14. Same as Figure S12C but showing differences in burned are fraction predicted by CMIP6 ESMs and those based on GFED estimates. Note that this comparison was restricted to a smaller subset of models.

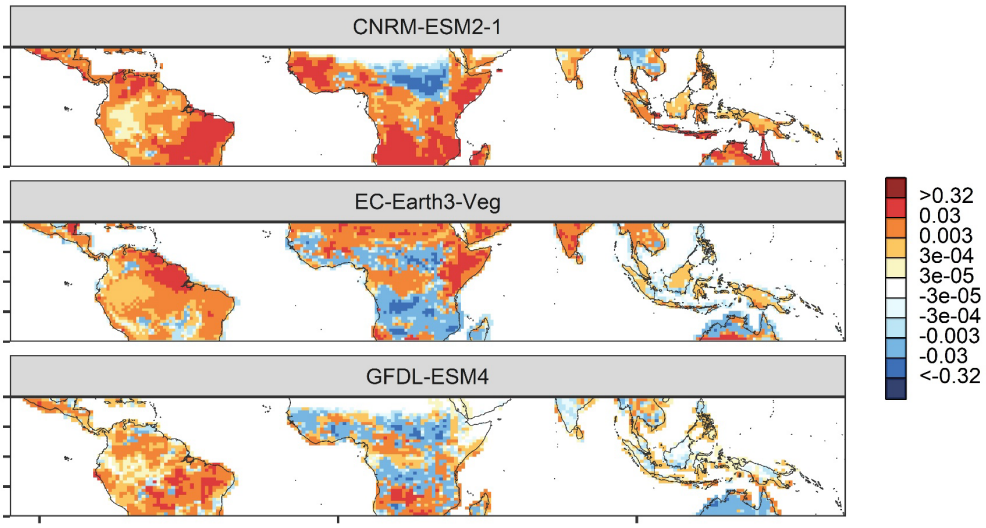

Fig. S15. Timing of the seasonal peak in fires (i.e., month with the highest carbon emission due to fires) in the Neotropics based on remote sensing data (GFED4s) and from CMIP6 ESMs historical simulations (1997-2014). Note that EC-Earth3-Veg and MRI-ESM2-0 models simulate fires on an annual basis and were not included.

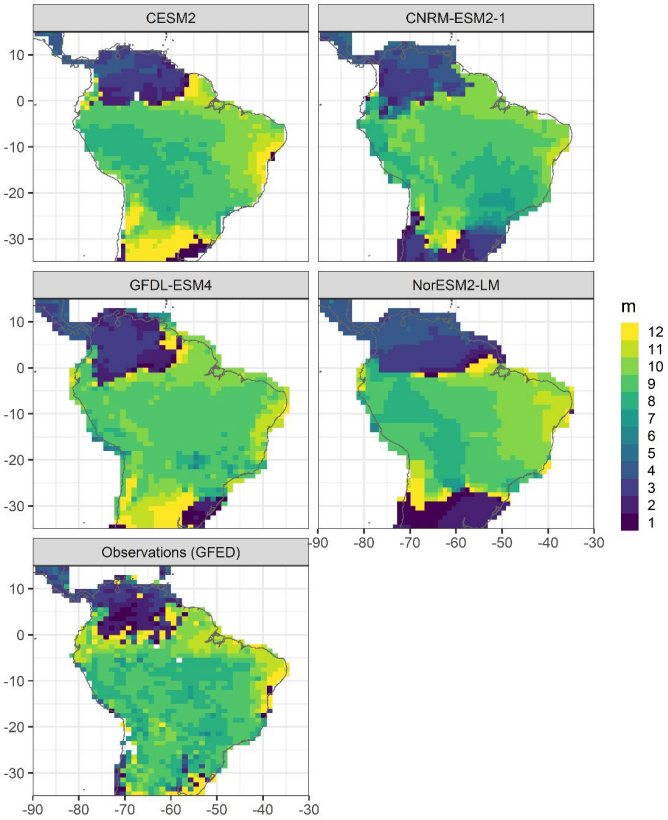

Fig. S16. Maximum absolute correlation coefficient *r* between annual changes in fire carbon emissions (kg C m^{-2} yr^{-1}) and lagged values of ONI (˚C) in CMIP6 models and in observations during 1997-2014 (GFED4s fire emissions and ONI values calculated by NOAA Climate Prediction Center).

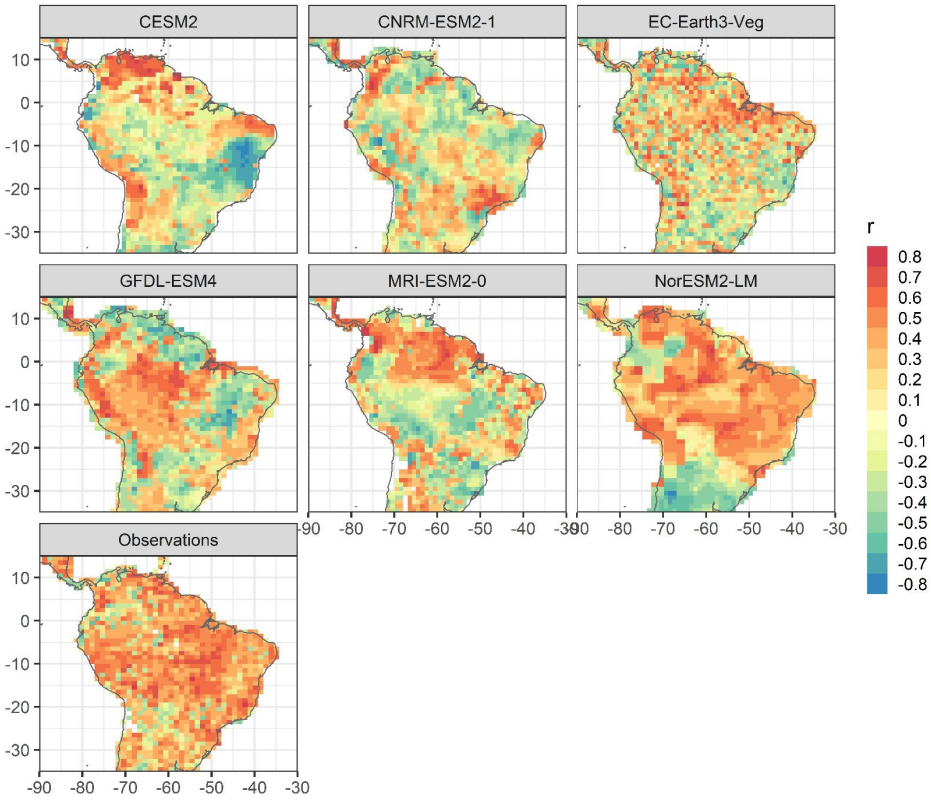

Fig. S17. Maximum absolute correlation coefficient *r* between annual changes in fire carbon emissions (kg C m^{-2} yr^{-1}) and lagged values of AMO (˚C) in CMIP6 models and in observations during 1997-2014 (GFED4s fire emissions and AMO values calculated by NOAA Climate Prediction Center).

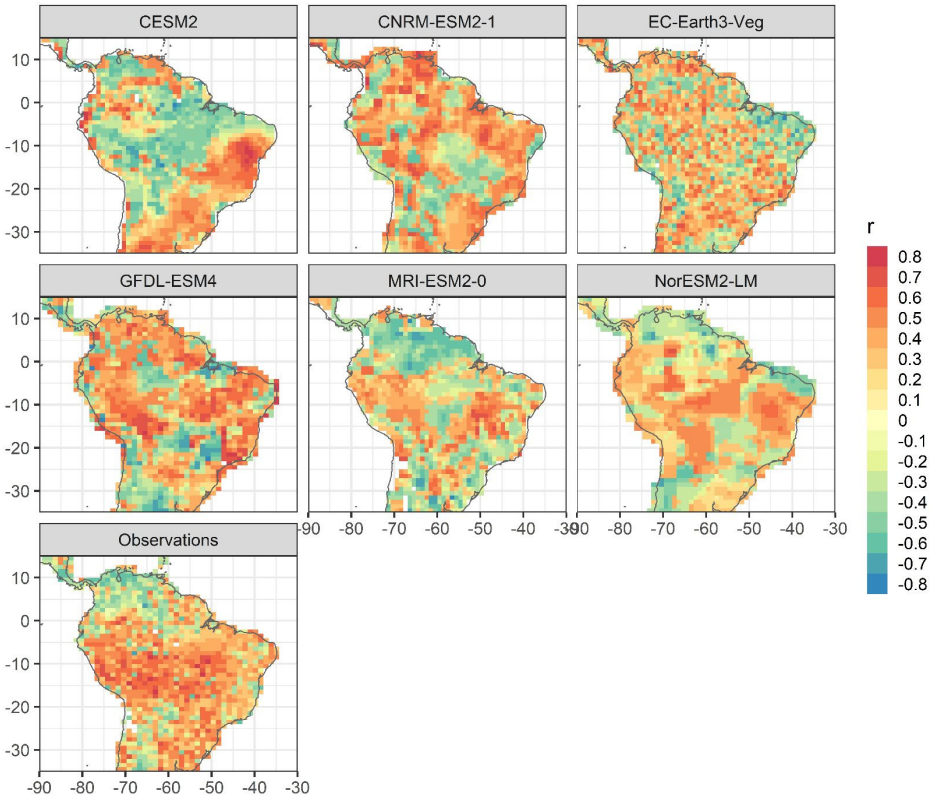

Fig. S18. Fire carbon emissions (kg C m^{-2} yr^{-1}) predicted by the phenomenological model based on the effect of AMO and ONI on tropical fires *vs* fire emissions simulated by CMIP6 ESMs. The last panel corresponds to the same relationship based on observations. As detailed in Methods, AMO and ONI indices were calculated for each dataset —both ESM output and observations— following the methods developed by NOAA Climate Prediction Center. Similarly, we fitted the phenomenological model developed by ref. (23) for each dataset optimizing the lagged effect of ONI and AMO on predicted fires. Each panel shows a two dimensional density plot calculated using logarithmic bins. The correlation coefficient *r* is detailed for each model in the upper left corner. Note that we added a minimum fire carbon emissions rate of 10^{-5} kg C m^{-2} yr^{-1} to retain grid cells with zero emissions after taking decimal logarithms.

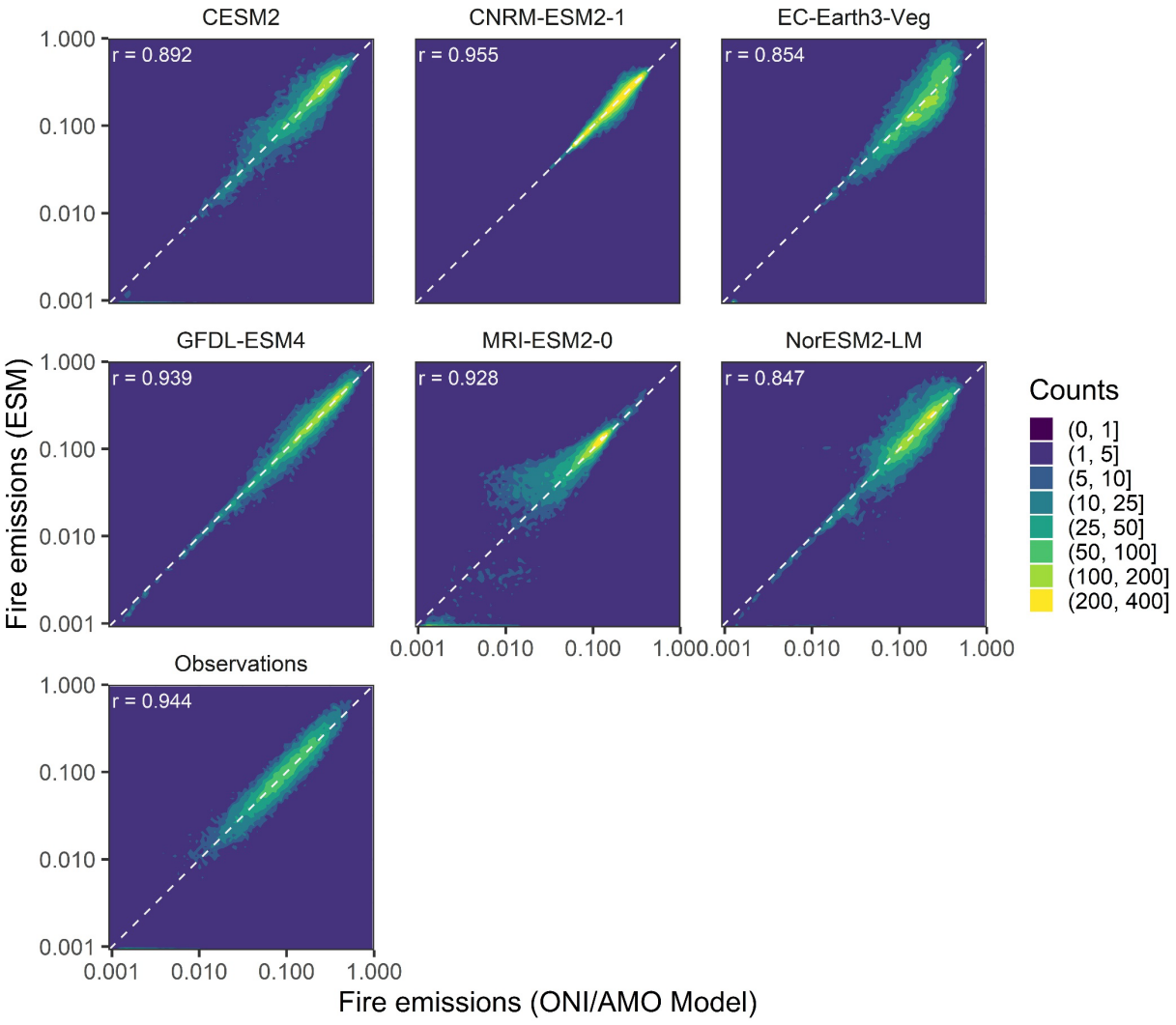

Fig. S19. Projected distribution of the relative rates of biomass increase (r_{Bm}, yr^{-1}) based on changes in annual woody biomass for the Amazon in simulations of CMIP6 models under scenario SSP5-8.5 (2015-2100).

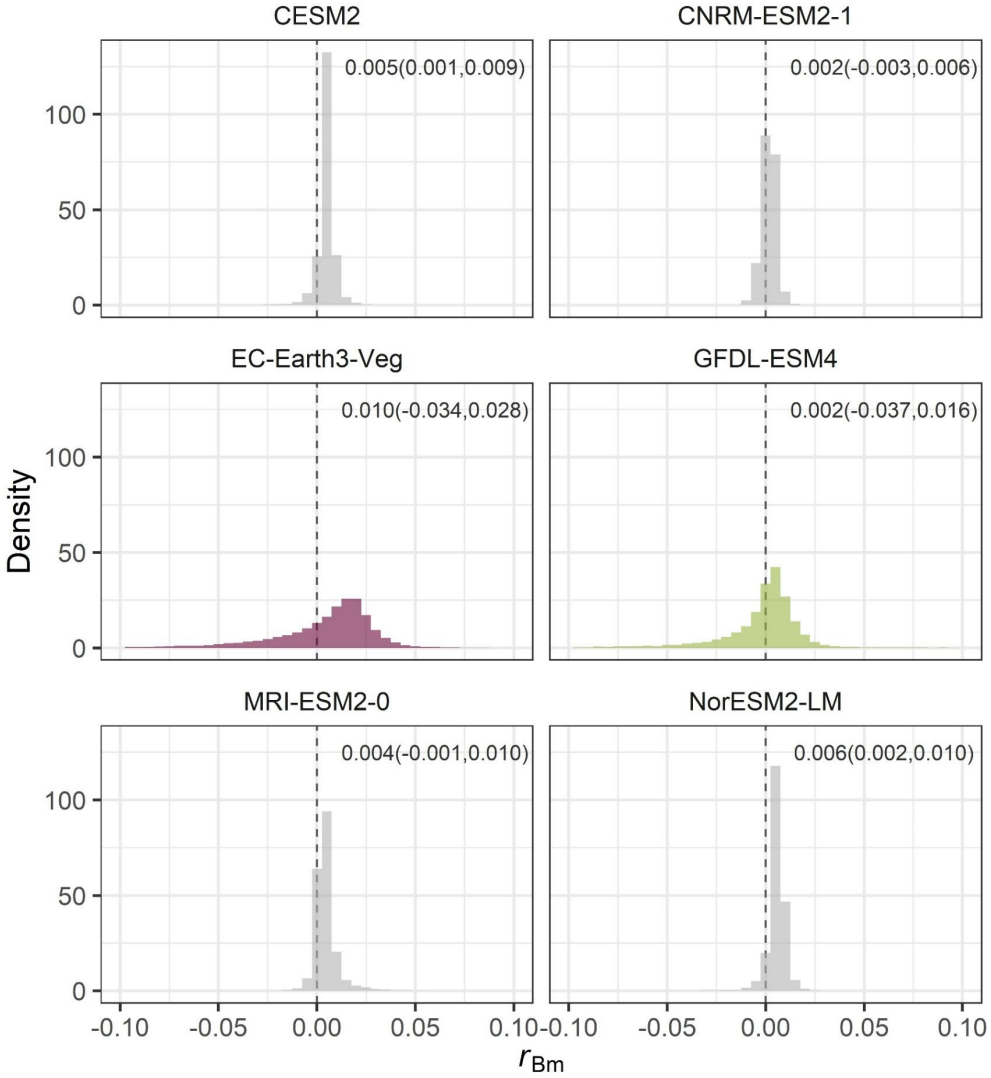

Fig. S20. Relationship between positive relative rates of biomass increase (r_{Bm}, yr^{-1}) and woody biomass (kg C m^{-2}) in EC-Earth3-Veg and GFDL-ESM4.1 simulations for Amazon grid cells under scenario SSP5-8.5.

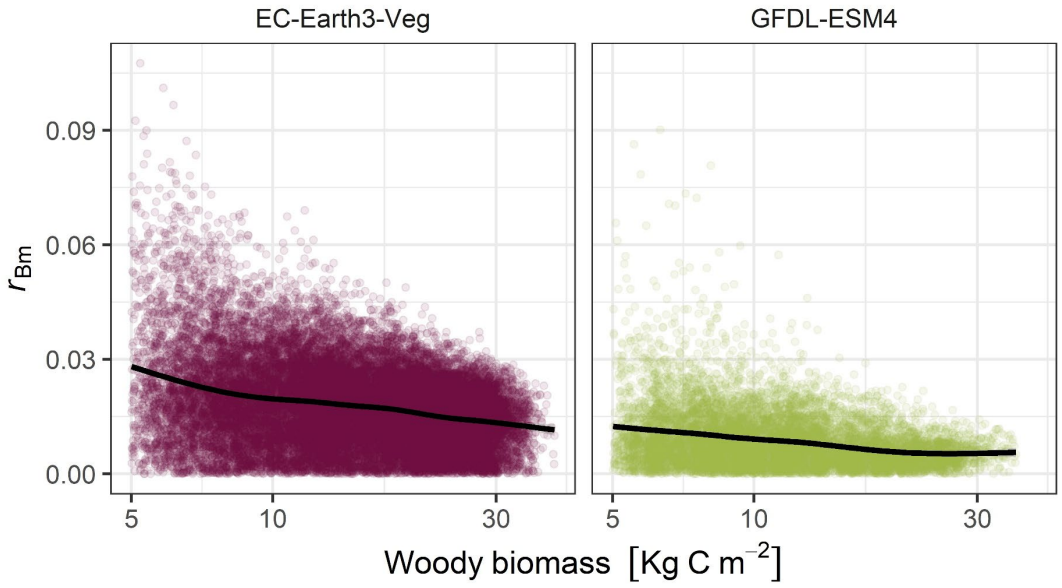

Fig. S21. Projections of tree biomass and grass fraction in the Neotropics based on EC-Earth-Veg simulation under scenario SSP5-8.5. (a) Time series plot similar to figure 2B in the main text. Orange lines (rug) along the abscissa correspond to high carbon emissions due to fires. Here, the purple segments on top of trends in tree biomass for each cell (green lines), highlight corresponding losses in years with high fires. (b) Time series of the fraction of grasses in each grid cell during the simulation. Note that these data are based on pooled diagnostics over vegetation and land use types.

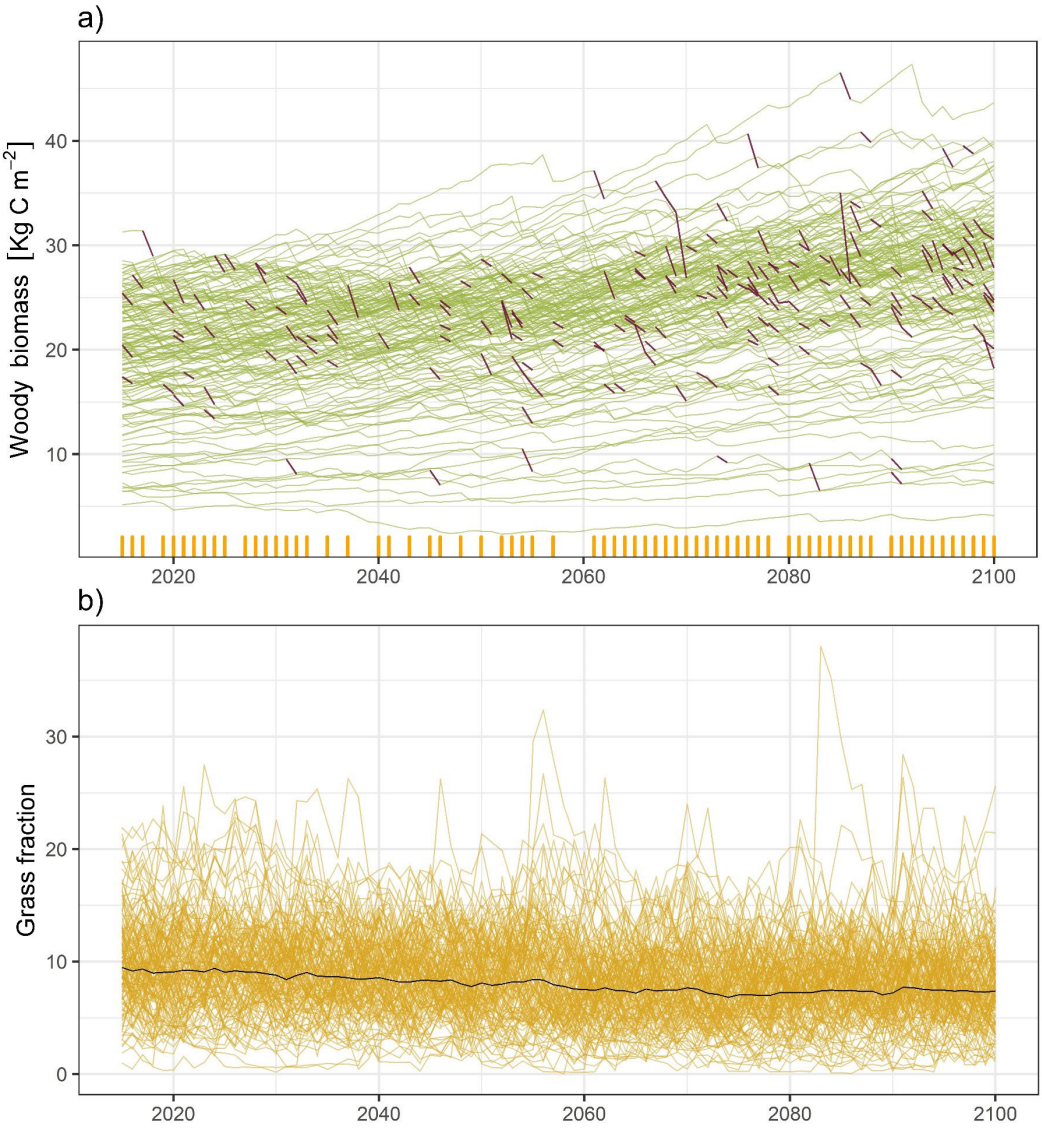

Fig. S22. Projected distribution of the net change in Amazon woody biomass between 2015 and 2100, $\Delta Bm_{2100\text{-}2015}$, in simulations of CMIP6 models under scenario SSP5-8.5.

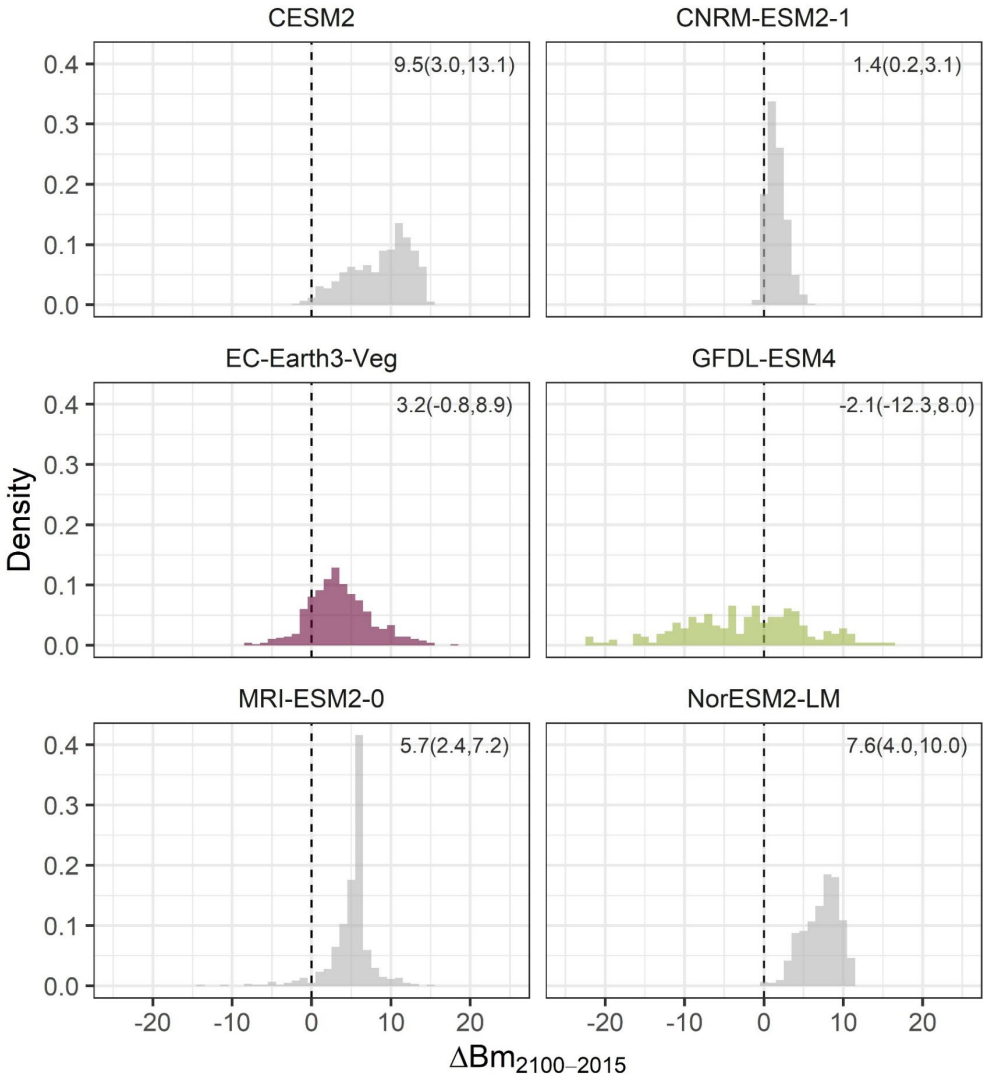

Fig. S23. Change in total tree biomass (yr^{-1}) for simulations of natural tropical forests dynamics with GFDL-ESM4.1 under scenarios SSP1-2.6 and SSP5-8.5. Increases and decreases in biomass are expressed as an instantaneous rate of change based on the change in biomass between 2015 and 2100.

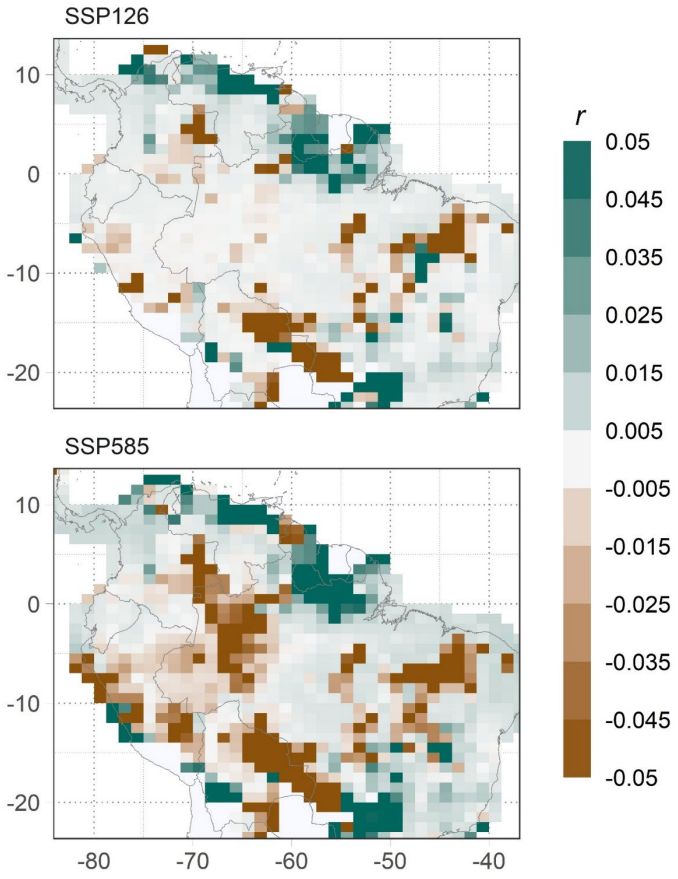

Fig. S24. Same as figure 2B in the main text, but featuring time series of projected total tree biomass (kg C m^{-2}) in the Neotropics simulated under scenario SSP5-8.5 in a global experiment forcing GFDL-ESM4.1 with the sea surface temperature fields simulated by EC-Earth3-Veg. Each line corresponds to the dynamics of natural tropical forests in individual grid cell locations. Trajectories showing a decrease in total biomass are highlighted with a purple hue.

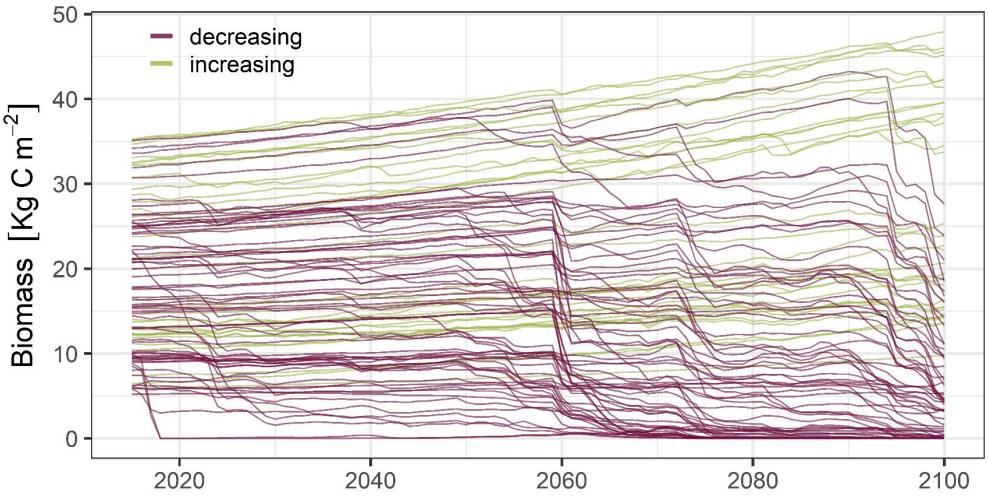

Fig. S25. Projected time series of tropical tree (green) and grass (yellow) biomass for selected grid cells in the Amazon where forest biomass collapsed in GFDL-ESM4.1 global simulation under emission scenario SSP5-8.5. The series were normalized to a 0-1 range to ease the comparison between vegetation types but also across cells of varying biomass. Orange lines (rug) along the abscissa indicate years with high carbon emissions due to fires.

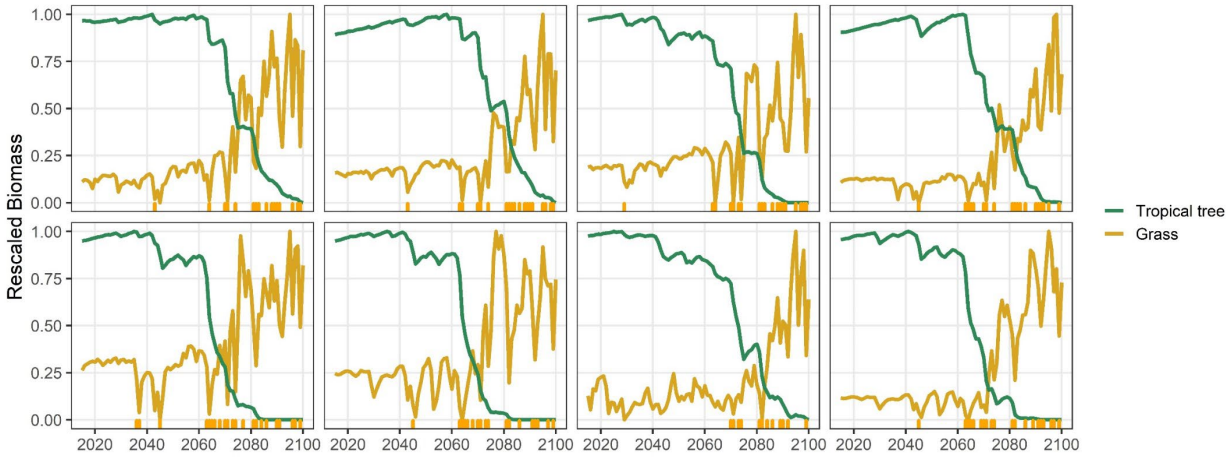

Supplementary Text.

Overview of vegetation dynamics in GFDL-ESM4.1 and EC-Earth-Veg

The development of the terrestrial components of GFDL-ESM4.1 and EC-Earth-Veg has its roots on forest gap models and shares a mechanistic approach to modeling vegetation dynamics. They also reflect slightly different solutions to the challenge of scaling local plant dynamics and interactions to simulating vegetation dynamics at large scales.

Both models follow the fate of a set of age cohorts composed by identical individuals that belong to a given species or vegetation type (plant functional type, PFT). Several cohorts coexist and interact within a patch or tile. Population dynamics and ecosystem patterns emerge from the basic processes of individual growth, reproduction and mortality, and from differences in physiological performance associated with plant competition for light and water resources. Each model grid cell contains a mosaic of tiles with different vegetation structure, which can result from the effects of land use or natural disturbance regime. This approach enables the emergence of heterogeneous, dynamic landscapes in response to climate change and land use scenarios like those provided by CMIP6.

GFDL-ESM4.1 and EC-Earth-Veg differ however in multiple aspects. First, they differ in the implementation of vertical vegetation structure and light competition among different kinds of plants within and among each canopy layer. GFDL-ESM4.1 adopts the perfect plasticity approximation (PPA) which assumes that plants will grow their canopies to capture available light[24,25]. It represents vertical vegetation structure as discrete layers with a number of cohorts occupying that layer. PPA assumes that all plants within each vertical layer receive the same down radiation from the atmosphere or a layer above and the same reflected radiation from the ground or layer below. However, each cohort absorbs different amounts of radiation depending on cohort leaf area index and leaf optical properties. As a result, the energy balance is separately computed for each cohort and canopy layer in GFDL-ESM4.1.

The alternative approach of EC-Earth-Veg calculates light extinction through the canopy accounting for the cumulated LAI above each canopy depth, so available light varies continuously[12,26]. The model simulates competition for light due to crown overlap following the patch-based scheme in LPJ-GUESS[11]. Light reaching the ground, above a minimum threshold, is available to a separate layer of grasses. Incoming PAR is partitioned among cohorts based on their relative height and LAI, which enables the implementation of asymmetric light competition and the effect of intra and interspecific shading on photosynthetic rates. The energy balance is based on the assumption of a continuous canopy and differs between high and low vegetation dependent on roughness length.

In the two models plant cohorts have access to vertically distributed soil water in a tile, which is balanced by runoff and evaporation to the atmosphere. GFDL-ESM4.1 recently incorporated the adaptive response of stomata to limiting water that combines constraints on carbon acquisition and hydraulic impairment[27]. On the other hand, EC-Earth-Veg implements plant competition for nitrogen[11]. Light and water limitation explicitly modulate recruitment in EC-Earth-Veg through vegetation type specific tolerance thresholds[26], while fluctuations in early growth and survival are an emergent process in GFDL-ESM4.1[17].

At the tile level, the models also differ in that GFDL-ESM4.1 simulates dynamic patches of varying size that split, for instance, following a perturbation to accommodate changes in land cover[28], while EC-Earth-Veg simulates a large number of fixed size patches that reminisces a collection of independent gap models[11]. In EC-Earth-Veg, the water cycle is loosely coupled to the rest of the model and locally dominant

vegetation determines hydrological processes[12], while the water cycle is closely coupled in GFDL-ESM4.1 by design[29].

With respect to the impact of fire disturbances, GFDL-ESM4.1 implements daily fires that can prompt tile splitting and lead to the formation of new tiles with a reduced biomass and altered vegetation composition and structure. In EC-Earth3-Veg, fires are simulated with a yearly time step and prompt biomass combustion and mortality of trees inhabiting the affected tile. GFDL-ESM4.1 includes unmanaged lands as natural primary and secondary vegetation (including fire affected tiles), while EC-Earth-Veg considers one natural tile type with a subset of up to 10 woody and 2 herbaceous PFTs, determined by bioclimatic envelope, co-occurring and interacting at patch scale. For the Amazonian focus area of this study, three PFTs – tropical raingreen trees, tropical evergreen trees, and C4 grasses – are important. Only three woody and two herbaceous vegetation types are considered in GFDL-ESM4.1.

This set of differences reflect alternative approaches and choices to face the challenge of translating individual plant processes and interactions to the simulation of global vegetation dynamics. In both models forest recovery dynamics emerge from the interaction of several processes, including low atmosphere and soil dynamics. Our study highlights the distinct impact of fires on tiles and the postfire colonization and competitive dynamics. However, identifying the relative contributions of each single process to differences in the models' respective outputs is extremely complicated and would require a battery of sensitivity experiments that extends beyond the scope of the current contribution.

GFDL-ESM4.1 fire model

GFDL-ESM4.1 implements the fire model FINAL[15], with later modifications to include multiday burning and enhanced fire spread rate through forest crowns[16], and to adapt it to the presence of multiple cohorts within each vegetation tile[18].

To diagnose the causes underlying the projected increase in the impact of fire disturbances in the Amazon in GFDL-ESM4.1 experiments under scenario SSP5-8.5, we focused on the set of factors that determine the emergence of fires in the model. The number of fires in a given cell results from the product of the number of ignitions, I_{tot} [number per km^2], and the probability that they become a fire, p_{fire},

$$N_{fire} \sim I_{tot} \times p_{fire} = (I_n + I_a) \times (f_T \times f_{PD} \times f_{AGB} \times f_{RH} \times f_\theta)$$

where the number of ignitions is the sum of anthropogenic ignitions, I_a, that depends on human population density, and natural ignitions, I_n, that vary with latitude and with the density of lightning flashes. The probability of fire ignitions varied during the simulation to reflect changes in human population density prescribed on each SSP, although such scenarios consider minor changes in population density in sparsely populated areas like the Amazon. GFDL-ESM4.1 features lighting strikes as the single source of natural ignitions based on the empirical model by ref. (30), which gives a seasonal climatology of lightning flashes as a function of latitude.

The probability of an ignition to becoming a fire, p_{fire}, modulates the number of fires through a series of suppressing fire factors that account for the effect of canopy temperature, T[°C], human population density, PD [people km^{-2}], above ground biomass, AGB [kg C m^{-2}] (heartwood, sapwood, labile carbon, live leaf and leaf litter), relative humidity, RH and soil moisture, θ. The shape of each of these factors was parameterized in most cases using a Gompertz function to allow a sigmoid, threshold like response (ref. 15 for a detailed description).

The likelihood and impact of fires depend on the amount of fuel accumulated in a given tile. Litter characteristics and composition are important to predict fire behavior[31]. In GFDL-ESM4.1, decomposing tissues from dead individuals, together with tissue turnover result in a net flux of carbon to the soil[28]. The contribution of different materials to fuel classes is parameterized implicitly[16]. The dryness of the necromass varies with environmental conditions, but it is not inherited from the state of the living plant (see ref. 32 for an alternative approach).

The areal extent affected by a fire is calculated assuming that fires have an elliptical shape determined by prevailing winds, with a maximum rate of spread that accounts for atmospheric and soil moisture conditions, and for vegetation and fuel composition. The calculation incorporates an extra term to account for the faster spread of high-intensity crown fires[16], which was separately parameterized for boreal, temperate and tropical regions. Burned area is also adjusted to account for the impact of landscape fragmentation in fire spread[33].

The impact of fires on vegetation combines partial biomass loss and direct mortality. The fraction of biomass lost depends on combustion rates that differ among species and tissues, but are independent of plant size. In this way, all individuals of a given species loss the same fraction of biomass, and thus the survival of small individuals becomes compromised with respect to large trees, which retain high potential for recovering from a fire. The additional mortality term is also species-specific but does not vary with

plant size or any other trait. Such an approach is conservative and does not account for known differences in fire sensitivity among plant life stages[32] or due to traits like bark thickness[34].

In GFDL-ESM4.1, fires affecting large areas (BA ≥ 1 Km^2) trigger the formation of disturbed patches with reduced tree dominance to mimic real world fire scars and their recovery after the disturbance. Succession is an emergent behavior that follows with local recovery, seed dispersal and colonization, though conditions in newly disturbed patches tend to favor certain vegetation types like grasses. The model implements universal dispersal within grid cells and it does not account for the potential effect of dispersal limitation on larger burned areas. We lack appropriate data to independently assess each of these processes, although they contribute to the ability of the model to reproduce large scale fire metrics.

References

1 Danabasoglu, G. NCAR CESM2 model output prepared for CMIP6 ScenarioMIP ssp585. doi:10.22033/ESGF/CMIP6.7768 (2019).

2 Li, F., Levis, S. & Ward, D. S. Quantifying the role of fire in the Earth system – Part 1: Improved global fire modeling in the Community Earth System Model (CESM1). *Biogeosciences* **10**, 2293-2314, doi:10.5194/bg-10-2293-2013 (2013).

3 Li, F., Zeng, X. D. & Levis, S. A process-based fire parameterization of intermediate complexity in a Dynamic Global Vegetation Model. *Biogeosciences* **9**, 2761-2780, doi:10.5194/bg-9-2761-2012 (2012).

4 Lawrence, D. M. *et al.* The Community Land Model Version 5: Description of New Features, Benchmarking, and Impact of Forcing Uncertainty. *Journal of Advances in Modeling Earth Systems* **11**, 4245-4287, doi:https://doi.org/10.1029/2018MS001583 (2019).

5 Seland, Ø. *et al.* NCC NorESM2-LM model output prepared for CMIP6 ScenarioMIP ssp585. doi:10.22033/ESGF/CMIP6.8319 (2019).

6 Voldoire, A. CNRM-CERFACS CNRM-ESM2-1 model output prepared for CMIP6 ScenarioMIP ssp585. doi:10.22033/ESGF/CMIP6.4226 (2019).

7 Delire, C. *et al.* The Global Land Carbon Cycle Simulated With ISBA-CTRIP: Improvements Over the Last Decade. *Journal of Advances in Modeling Earth Systems* **12**, e2019MS001886, doi:https://doi.org/10.1029/2019MS001886 (2020).

8 Thonicke, K., Venevsky, S., Sitch, S. & Cramer, W. The role of fire disturbance for global vegetation dynamics: coupling fire into a Dynamic Global Vegetation Model. *Global Ecology and Biogeography* **10**, 661-677, doi:https://doi.org/10.1046/j.1466-822X.2001.00175.x (2001).

9 Séférian, R. *et al.* Evaluation of CNRM Earth System Model, CNRM-ESM2-1: Role of Earth System Processes in Present-Day and Future Climate. *Journal of Advances in Modeling Earth Systems* **11**, 4182-4227, doi:https://doi.org/10.1029/2019MS001791 (2019).

10 Consortium, E. C.-E. EC-Earth-Consortium EC-Earth3-Veg model output prepared for CMIP6 ScenarioMIP ssp585. doi:10.22033/ESGF/CMIP6.4914 (2019).

11 Smith, B. *et al.* Implications of incorporating N cycling and N limitations on primary production in an individual-based dynamic vegetation model. *Biogeosciences* **11**, 2027-2054, doi:10.5194/bg-11-2027-2014 (2014).

12 Döscher, R. *et al.* The EC-Earth3 Earth System Model for the Climate Model Intercomparison Project 6. *Geosci. Model Dev.* **15**, 2973–3020, doi:10.5194/gmd-15-2973-2022 (2022).

13 John, J. G. *et al.* NOAA-GFDL GFDL-ESM4 model output prepared for CMIP6 ScenarioMIP. doi:10.22033/ESGF/CMIP6.1414 (2018).

14 Krasting, J. P. *et al.* NOAA-GFDL GFDL-ESM4 model output prepared for CMIP6 CMIP historical. doi:10.22033/ESGF/CMIP6.8597 (2018).

15 Rabin, S. S. *et al.* A fire model with distinct crop, pasture, and non-agricultural burning: use of new data and a model-fitting algorithm for FINAL.1. *Geosci. Model Dev.* **11**, 815-842, doi:10.5194/gmd-11-815-2018 (2018).

16 Ward, D. S., Shevliakova, E., Malyshev, S. & Rabin, S. Trends and Variability of Global Fire Emissions Due To Historical Anthropogenic Activities. *Global Biogeochemical Cycles* **32**, 122-142, doi:https://doi.org/10.1002/2017GB005787 (2018).

17 Martínez Cano, I. *et al.* Allometric constraints and competition enable the simulation of size structure and carbon fluxes in a dynamic vegetation model of tropical forests (LM3PPA-TV). *Global Change Biology* **26**, 4478-4494, doi:10.1111/gcb.15188 (2020).

18 Shevliakova, E. *et al.* The land component LM4.1 of the GFDL Earth system model ESM4.1: biophysical and biogeochemical processes and interactions with climate. ((in revision)).

19 Yukimoto, S. *et al.* MRI MRI-ESM2.0 model output prepared for CMIP6 ScenarioMIP ssp585. doi:10.22033/ESGF/CMIP6.6929 (2019).
20 Yukimoto, S. *et al.* The Meteorological Research Institute Earth System Model Version 2.0, MRI-ESM2.0: Description and Basic Evaluation of the Physical Component. *J. Meteorological Soc. Jpn. Ser. II* **97**, 931-965, doi:10.2151/jmsj.2019-051 (2019).
21 Brienen, R. J. W. *et al.* Long-term decline of the Amazon carbon sink. *Nature* **519**, 344-348, doi:10.1038/nature14283 (2015).
22 Avitabile, V. *et al.* An integrated pan-tropical biomass map using multiple reference datasets. *Global Change Biology* **22**, 1406-1420, doi:https://doi.org/10.1111/gcb.13139 (2016).
23 Chen, Y. *et al.* Forecasting Fire Season Severity in South America Using Sea Surface Temperature Anomalies. *Science* **334**, 787-791, doi:10.1126/science.1209472 (2011).
24 Strigul, N., Pristinski, D., Purves, D., Dushoff, J. & Pacala, S. Scaling from trees to forests: tractable macroscopic equations for forest dynamics. *Ecological Monographs* **78**, 523-545, doi:https://doi.org/10.1890/08-0082.1 (2008).
25 Weng, E. S. *et al.* Scaling from individual trees to forests in an Earth system modeling framework using a mathematically tractable model of height-structured competition. *Biogeosciences* **12**, 2655-2694, doi:10.5194/bg-12-2655-2015 (2015).
26 Smith, B., Prentice, I. C. & Sykes, M. T. Representation of vegetation dynamics in the modelling of terrestrial ecosystems: comparing two contrasting approaches within European climate space. *Global Ecology and Biogeography* **10**, 621-637, doi:https://doi.org/10.1046/j.1466-822X.2001.t01-1-00256.x (2001).
27 Wolf, A., Anderegg, W. R. L. & Pacala, S. W. Optimal stomatal behavior with competition for water and risk of hydraulic impairment. *Proceedings of the National Academy of Sciences* **113**, E7222-E7230, doi:10.1073/pnas.1615144113 (2016).
28 Shevliakova, E. *et al.* Carbon cycling under 300 years of land use change: Importance of the secondary vegetation sink. *Global Biogeochemical Cycles* **23**, doi:https://doi.org/10.1029/2007GB003176 (2009).
29 Dunne, J. P. *et al.* The GFDL Earth System Model Version 4.1 (GFDL-ESM 4.1): Overall Coupled Model Description and Simulation Characteristics. *Journal of Advances in Modeling Earth Systems* **12**, e2019MS002015, doi:https://doi.org/10.1029/2019MS002015 (2020).
30 Prentice, S. A. & Mackerras, D. The Ratio of Cloud to Cloud-Ground Lightning Flashes in Thunderstorms. *Journal of Applied Meteorology and Climatology* **16**, 545-550, doi:10.1175/1520-0450(1977)016<0545:TROCTC>2.0.CO;2 (1977).
31 Cochrane, M. A. Fire science for rainforests. *Nature* **421**, 913-919, doi:10.1038/nature01437 (2003).
32 De Faria, B. L. *et al.* Current and future patterns of fire-induced forest degradation in Amazonia. *Environmental Research Letters* **12**, 095005, doi:10.1088/1748-9326/aa69ce (2017).
33 Pfeiffer, M., Spessa, A. & Kaplan, J. O. A model for global biomass burning in preindustrial time: LPJ-LMfire (v1.0). *Geosci. Model Dev.* **6**, 643-685, doi:10.5194/gmd-6-643-2013 (2013).
34 Brando, P. M. *et al.* Fire-induced tree mortality in a neotropical forest: the roles of bark traits, tree size, wood density and fire behavior. *Global Change Biology* **18**, 630-641, doi:https://doi.org/10.1111/j.1365-2486.2011.02533.x (2012).